

Article

# Research on Airspace Conflict Detection Method Based on Spherical Discrete Grid Representation

Kai Qu, Guhao Zhao \*, Yarong Wu and Liang Tong 

Air Traffic Control and Navigation College, Air Force Engineering University, Xi'an 710051, China; graduateqk1@163.com (K.Q.)

\* Correspondence: zghlupin@163.com

**Abstract:** With the continuous development of general aviation, the contradiction between the air demand of general aviation low-altitude airspace and civil aviation routes is sharp. The difficulty of airspace planning is complex and changeable, and the existing working mode of simply using computer mapping and manually finding airspace conflict contradictions can no longer meet the large-scale air use demand. In response to the existing spatial representation model of longitude and latitude grid, which has large grid deformation in high latitude areas, and the problem of slow computation speed of the conflict detection (CD) algorithm that determines whether the airspace boundary coordinates overlap, we propose a grid model that represents airspace with a spherical rhombic discrete grid of positive icosahedron and design a matrix-based digital representation method of airspace, which uses matrix product operation. The matrix product operation is used to quickly determine whether there is a conflict between airspace and airspace and between airspace and routes.

**Keywords:** airspace conflict detection; spherical discrete grid; matrix operation



**Citation:** Qu, K.; Zhao, G.; Wu, Y.; Tong, L. Research on Airspace Conflict Detection Method Based on Spherical Discrete Grid Representation. *Appl. Sci.* **2023**, *13*, 6493. <https://doi.org/10.3390/app13116493>

Academic Editor: Rosario Pecora

Received: 18 April 2023

Revised: 21 May 2023

Accepted: 24 May 2023

Published: 26 May 2023



**Copyright:** © 2023 by the authors. Licensee MDPI, Basel, Switzerland. This article is an open access article distributed under the terms and conditions of the Creative Commons Attribution (CC BY) license (<https://creativecommons.org/licenses/by/4.0/>).

## 1. Introduction

As the carrier of aviation activities, airspace is limited and non-renewable, which decides that only one aviation user can occupy one airspace at the same time and the same height, and in the same range. Therefore, with the rapid increase of air users in public transport aviation, general aviation, military aviation, and so on, frequent use of airspace leads to severe aviation safety and collision situations. How to use airspace safely and efficiently on a large scale has become a major problem for air traffic control departments.

For the study of the airspace CD problem, the traditional solution is to perform cross-operations on the longitude and latitude ranges of airspace to determine whether there is a conflict. This method is complex, computationally intensive, and time-consuming, and is only applicable to the detection of small-scale airspace conflicts. Moreover, the longitude and latitude grids have large deformation in high latitudes and cannot accurately characterize the airspace range. At the same time, the traditional solution cannot encode airspace data, and it is not convenient for information storage and management in the process of airspace control.

In order to solve the above problems, Sahr [1] proposed the discrete global grid system (DGGS), which solves the problem that the grid becomes larger with the higher latitude. White D [2] uses a variety of projection methods to solve the problem of projecting regular icosahedron onto the Earth's surface. Gregory M J et al. [3] obtained that the evaluation index of a regular icosahedron is better than that of a regular octahedron according to the two standard evaluation indexes of grid distance and the "grid wall midpoint" criterion. Ben Jin et al. [4] establishes the corresponding relationship between plane and sphere on the basis of a regular icosahedron. Zhou Liangchen et al. [5] proposed a spherical diamond discrete grid regular icosahedron dissection method, the resulting grid at different levels,

angular deformation, and area deformation are kept to a minimum. Lin Bingxian et al. [6] studied the coding model and its mapping method based on a regular icosahedral spherical diamond discrete grid and realized the conversion method between grid coding and geographical coordinates.

At present, with the development of spatial geographic grid research, there are more and more CD methods based on gridded airspace. Jardin M [7] proposed a CD algorithm based on a four-dimensional spatial and temporal grid to represent aircraft trajectories in airspace, which determines whether there is a conflict by checking grid occupancy. S. Ruiz et al. [8] proposed a CD algorithm based on spatial data structure by storing the trajectory information in a square grid space and using a conflict detection method based on correlated spatial data structure as well as a CD method based on spatio-temporal data structure to achieve fast CD; Kuenz A [9] proposed a new 4D airspace modeling method that combines traffic, weather, restricted areas and other objects in 4D airspace for CD and disambiguation. Miao S et al. [10] proposed a new multi-level grid spatio-temporal index for a new low-altitude flight CD algorithm; Liu ZQ et al. [11] proposed a method to characterize the conflicting airspace based on the earth profile grid model and calculate the conflicting airspace using a multinomial tree structure; Gong W et al. [12] proposed a raster model-based airspace CD and deconfliction technique and established a numerical model of airspace conflict; Sui D et al. [13] established a deterministic CD and deconfliction module, used the R-tree algorithm with low time complexity to effectively reduce the number of comparisons between aircraft 4DTs, and proposed a Monte Carlo tree search algorithm; Cai M et al. [14] proposed a method to determine the airspace conflict by using the GJK algorithm to transform the airspace grid (AG) set into a coordinate set and by judging the inclusion relationship between the Minkowski difference set and the coordinate origin.

In this paper, a space coding representation model based on an icosahedral spherical rhombus discrete grid and a space CD method based on matrix Hadamard product operation are established. A set of methods for transforming the longitude and latitude of the airspace boundary to the positioning code is designed, which can uniquely and accurately locate the AG code. Realize that under different latitude and longitude, the grid scale is moderate, suitable for airspace representation (AR) and matrix operation, and there is no obvious deformation. In this paper, the method of matrix Hadamard product is used to calculate the airspace conflict, which solves the defect of inaccurate spatial representation of the existing detection method. It achieves the goals of global coding of airspace and the accuracy and security required for airspace CD, and provides a data basis for the implementation of subsequent airspace conflict resolution algorithms.

## 2. Determination of the Airspace Grid Subdivision System

The subdivision of global airspace in a certain way is the basis of AG, and the selection of different subdivision methods will lead to different calculation methods. Therefore, according to the characteristics of airspace conflict recognition, an appropriate way is selected to represent airspace.

### 2.1. Introduction of Typical Global Subdivision Schemes

Global discrete grid systems can be classified into four categories: equal longitude and latitude grid, variable longitude and latitude grid, adaptive spherical grid, and regular polyhedral grid [15].

#### (1) Equal longitude and latitude grid

Equal longitude and latitude grid is a kind of grid formed by interweaving longitude and latitude at fixed intervals on the Earth, which is the earliest and most widely used one of the Earth's space coordinate grids [16]. At present, there have been applications of equal longitude and latitude grid systems, including the U. S. military grid reference system (MGRS) and GARS grid [17]. As shown in Figure 1:

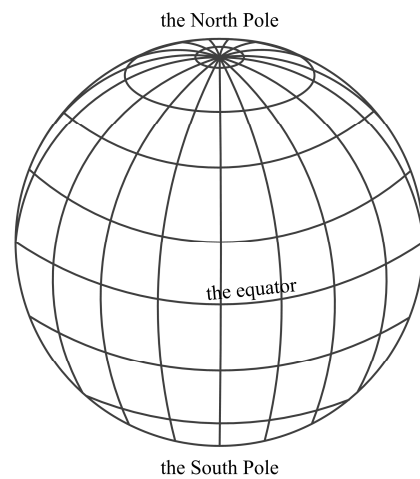


**Figure 1.** Equal longitude and latitude grid.

(2) Variable longitude and latitude grid

Variable longitude and latitude grids are subdivision schemes that change the longitude interval at different latitudes so that the area of gridded cells at the same level is approximately equal. This type of scheme trades off increased cell deformation and connection complexity for essentially the same area metric [18]. As shown in Figure 2:

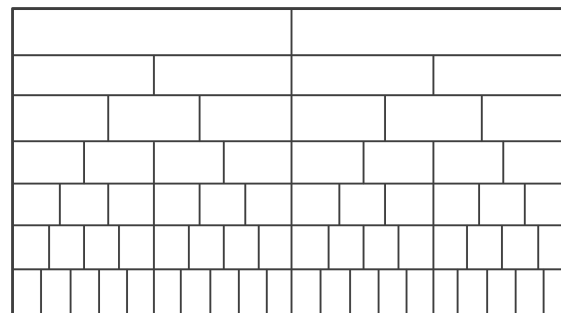


**Figure 2.** Variable longitude and latitude grid.

(3) Adaptive spherical grid

The adaptive spherical grid is not divided based on longitude and latitude but based on the solid elements on the sphere and some features of the solid [19]. In this method, the grid element is adaptively adjusted according to the solid data. Therefore, the adaptive spherical grid has better flexibility, meets the calculation needs of the mode requiring boundary fitting, and can complement other generation methods. As shown in Figure 3:

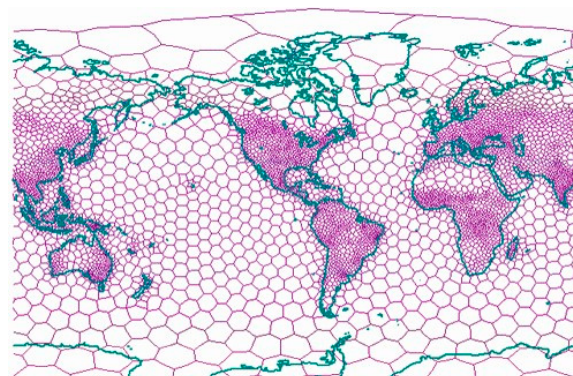


**Figure 3.** Adaptive spherical grid.

#### (4) Regular polyhedral grid

A regular polyhedron grid refers to connecting a sphere with a regular polyhedron, projecting all sides of the regular polyhedron onto the sphere to form spherical polygons [20], which will be used as the initial unit of the subdivision. Recursive subdivision will be carried out on this basis to form a grid model with good hierarchy, approximate uniformity, and global unity.

#### 2.2. Comparison of Airspace Grid Subdivision Systems

The design of AG requires unique shape, accuracy and coding mode, and the four mainstream subdivision schemes have their own advantages and disadvantages. Therefore, based on the actual needs of airspace planning, this paper compares the “Goodchild” grid criterion [21] to make it meet the needs of AG and facilitate subsequent matrix operations.

The drawbacks of the equal longitude and latitude grid and the variable longitude and latitude grid are that the area of the grid at high and low latitudes has a large deformation and degrades from rectangular to triangular at the poles, which does not meet the needs of AR.

Although the adaptive grid is flexible, the irregular shape of the grid makes it difficult to perform recursive subdivision and encoding, which causes great computational difficulties and is not suitable for AR.

Relatively speaking, the regular polyhedron grid can best meet the above requirements. First of all, the geometric shape of the regular polyhedron grid is approximately the same, and there will be no obvious change between high and low latitudes; secondly, the grid can carry out nesting and multi-level recursive division according to the same rules, so the grid is regular and easy to code; finally, there is a corresponding relationship between geographical coordinates and grid system and longitude and latitude coordinates can be converted into grid coding. The geometric structure of the diamond grid is simple and the direction is consistent [22], and the diamond grid can be regarded as a deformed square grid, which is suitable for matrix operation.

In summary, this paper selects a positive icosahedral rhombic grid for global subdivision and constructs an AG.

### 3. Construction of Airspace Grid Model Based on Icosahedron Spherical Rhombus Subdivision

#### 3.1. Construction of Subdivision Model

In the quadtree subdivision method based on the spherical diamond grid, the degree of grid deformation is mainly judged by the ratio of the long and short axes of the grid, the ratio of the maximum and minimum area, and the mean square error of the grid perimeter. The ratio of the long and short axes of the subdivided rhombus grid at each level remains basically unchanged at about 1.4, and the ratio of the long and short axes of the rest of the subdivision methods is greater than 2 and will change with the change of the subdivision level. The maximum and minimum area ratio of the icosahedral rhombic grid will not change with the increase of the grid subdivision level, and is constant at 1.3, which is also the best among various subdivision methods [23]. The grid has the advantages of compactness and continuity, and the grid unit has one and only one identification point. It conforms to the ideal grid subdivision evaluation criteria proposed by Goodchild M F [24] and is suitable for global multi-level subdivision and spatial coding.

According to the geometric properties of the icosahedron, there are three methods of placing the spherical surface. In order to facilitate the simplified transformation from latitude and longitude coordinates to coded coordinates, as well as subsequent grid division and coding, this paper uses the 0-degree meridian as the symmetry axis to place the method. Correspondence between icosahedron and sphere [25]. As shown in Figure 4:

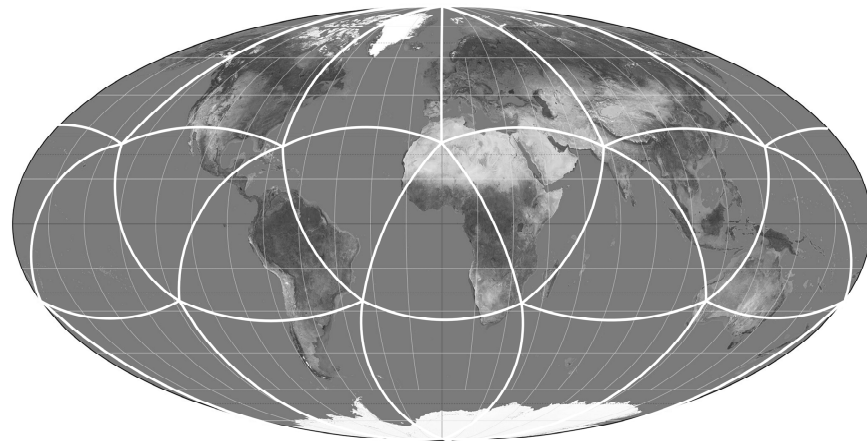


**Figure 4.** Placement method of spherical regular icosahedron.

For the great circle arc subdivision of the icosahedron, the spherical distance calculation methods include the great circle formula, the simplified great circle formula, and the Haversine formula. Compared with the accuracy of the above calculation methods, the great circle formula has a very serious rounding error under single precision, while the great circle formula The simplified formula of has a large error when the distance between the two poles or two points is large, and the precision of the Haversine formula is similar to that of the Cartesian coordinate system method, both of which are very high [26]. The distance  $D$  between two points on the sphere is obtained from Haversine’s formula, where  $\lambda$  denotes longitude,  $\varphi$  denotes latitude, and  $R$  is the radius of the Earth.

$$D = 2R \arcsin \left( \sqrt{\sin^2 \left( \frac{\varphi_2 - \varphi_1}{2} \right) + \cos(\varphi_1) \cos(\varphi_2) \sin^2 \left( \frac{\lambda_2 - \lambda_1}{2} \right)} \right) \quad (1)$$

The coordinates of the subdivision levels and boundary points and the edge lengths of the diamond grid are determined by calculation, and the correspondence between the scales of each level is shown in Table 1.

**Table 1.** Correspondence of each level of scale.

Subdivision Level	Rhombus Side Length/km	Number of Global Grids	Rhombic Spherical Area/km <sup>2</sup>	Distance from the Vertex of the Rhombus to the Opposite Side/km
0	7061	10	51,006,786	6115
1	3630	40	12,751,696	3057
2	1865	160	3,187,924	1529
3	960	640	796,981	765
4	480	2560	199,245	382
5	221	10,240	49,811	191
6	110	40,960	12,452	95
7	55	163,840	3113	47
8	28	655,360	778	24
9	14	2,621,440	194	12
10	7	10,485,760	48	6

The initial 10 rhombuses are at the 0th level, and the length of a single rhombus edge is about 7061 km according to the spherical arc length calculation formula, and the length of a single rhombus edge is about 7 km when dissecting to the 10th level, and the minimum distance of non-adjacent rhombus grids is one rhombus grid interval, i.e., the vertical distance from the rhombus vertex to the opposite edge is about 6 km. when CD, the

airspace is expanded by one layer, i.e., the interval of two enclosing The minimum distance is 11.94 km, which is greater than 10 km.

Therefore, the subdivision to the 10th level, which not only satisfies the minimum safe separation distance of the airspace, but also does not cause the grid deformation in different latitudes, and satisfies the required accuracy condition for the use of the AR grid.

### 3.2. Interchange of Coordinate Systems

(1) Conversion of longitude and latitude coordinates to spherical Cartesian coordinates;

The longitude and latitude coordinates of the airspace boundary points are transformed into spherical Cartesian coordinates. The longitude and latitude coordinates  $G$  (longitude  $\lambda$ , latitude  $\varphi$ ), the Earth's equatorial radius  $R$ , and the corresponding spherical Cartesian coordinates are  $C$  ( $X, Y, Z$ ), and the relationship from the longitude and latitude coordinates to the spherical Cartesian coordinates can be established by the spatial geometric relationship. As shown in Figure 5.

$$X = R \cos\left(\varphi \frac{\pi}{180}\right) \cos\left(\lambda \frac{\pi}{180}\right) \tag{2}$$

$$Y = R \cos\left(\varphi \frac{\pi}{180}\right) \sin\left(\lambda \frac{\pi}{180}\right) \tag{3}$$

$$Z = R \sin\left(\varphi \frac{\pi}{180}\right) \tag{4}$$

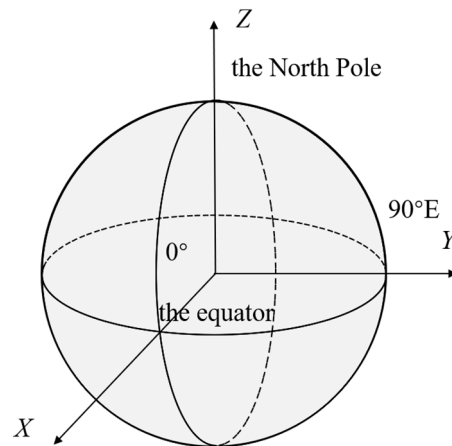


Figure 5. Schematic diagram of spherical Cartesian coordinates.

(2) Conversion of spherical Cartesian coordinates to longitude and latitude coordinates;

Since trigonometric functions have one-to-many situations in the range of 0–360°, there will be multiple solutions when converting from spherical Cartesian coordinates to longitude and latitude, so the specific coordinates need to be determined according to the positive and negative of spherical Cartesian coordinates during conversion. In addition to the north and south poles, the conversion relationship is as follows:

$$\alpha = \arctan\left(\left|\frac{Y}{X}\right|\right) \cdot \left(\frac{180}{\pi}\right) \tag{5}$$

$$\beta = \arctan\left(\frac{|Z|}{\sqrt{X^2 + Y^2}}\right) \cdot \left(\frac{180}{\pi}\right) \tag{6}$$

When  $X > 0, Y > 0$ ,  $\lambda$  is east longitude,  $\lambda = \alpha$ ;

When  $X < 0, Y > 0$ ,  $\lambda$  is east longitude,  $\lambda = \alpha + 90^\circ$ ;

When  $X > 0, Y < 0$ ,  $\lambda$  is west longitude,  $\lambda = \alpha$ ;

When  $X < 0, Y < 0$ ,  $\lambda$  is west longitude,  $\lambda = \alpha + 90^\circ$   
 When  $Z > 0$ ,  $\varphi$  is north latitude,  $\varphi = \beta$   
 When  $Z < 0$ ,  $\varphi$  is south latitude,  $\varphi = \beta$

### 3.3. Grid Coding Method

The description of the spatial location of the AG unit needs to be realized through geocoding. Hilbert curve has been proven to be a space-filled curve that can best maintain the local adjacency of space points [27].

Connect the midpoint of the opposite side of the rhombus grid to obtain four sub-rhombus. Set the four sub-rhombus as quadrants 0, 1, 2, and 3 respectively. Fill the quadrants with a Hilbert curve, and set them as I, II, III, and IV respectively, as shown in Figure 6. According to the Hilbert coding and state transfer mode of the initial diamond grid, the Hilbert coding and state transfer mode of the sub-diamond can be deduced [28]. By constructing multi-level Hilbert curves, the low-level curves of the AG can be formed by the translation or rotation of high-level curves through corresponding rules at each level of subdivision.

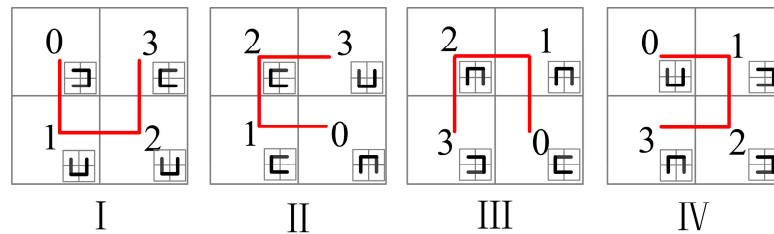


Figure 6. State transition mode of each quadrant of the Hilbert curve.

For example, in the case of level  $m$  and the current status is I, when point  $P$  is located in the quadrant with the number of binary value 01 (that is, sub-diamond number 1), the status of the next level can be deduced from the status transfer table as b. The number binary value 01 is used as the coding of the  $m$  level. On this basis, the coding and segmentation of the  $m + 1$  level are continued under the current status of II, and the code 0101 of the  $m + 1$  level is obtained. As shown in Figure 7.

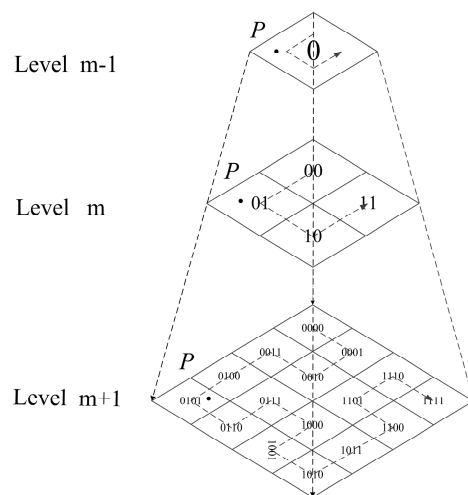


Figure 7. Mapping method of low order Hilbert curve to high order.

The representation of the target point consists of the following parts:

- The first part: the diamond code: the 0th level of the segmentation. Table 2 shows the longitude and latitude coordinates of the vertices of the regular icosahedron. Use binary to represent the serial number of the initial diamond, as shown in Figure 8:

**Table 2.** Longitude and latitude coordinates of the vertex of a regular icosahedron.

Vertice	Longitude	Latitute	Vertice	Longitude	Latitute
S0	0° E	90° N	S6	36° E	26.57° S
S1	0° E	26.57° N	S7	108° E	26.57° S
S2	72° E	26.57° N	S8	180° E	26.57° S
S3	144° E	26.57° N	S9	108° W	26.57° S
S4	144° W	26.57° N	S10	36° W	26.57° S
S5	72° W	26.57° N	S11	0° E	90° S

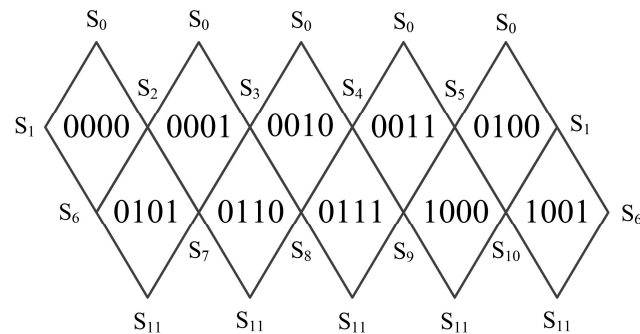


**Figure 8.** Ordinal number of initial rhombus position of the icosahedron.

- The second part: location code: the 1–3rd levels of segmentation. The grid quadtree is divided, the grid space is filled by the Hilbert curve, and the binary code is converted into Hilbert code;
- The third part: coordinate code: the 4–10th levels of segmentation. The grid quadtree is divided, and the grid space is filled by the Hilbert curve. The binary code is converted into Hilbert code, and then the Hilbert code is converted into  $(i, j)$  coordinates.

Take the longitude and latitude coordinates [7.29, 51.19] as an example, first, determine the diamond number of the point as 1, divide the grid to the 10th level, and obtain the binary code of 1–3rd levels of 000101, and the binary code of 4–10th levels of 10000011111000. According to the above method, the global unique representation of the target point is obtained, and the global code is [diamond code, location code, coordinate code]. As shown in Figure 9:

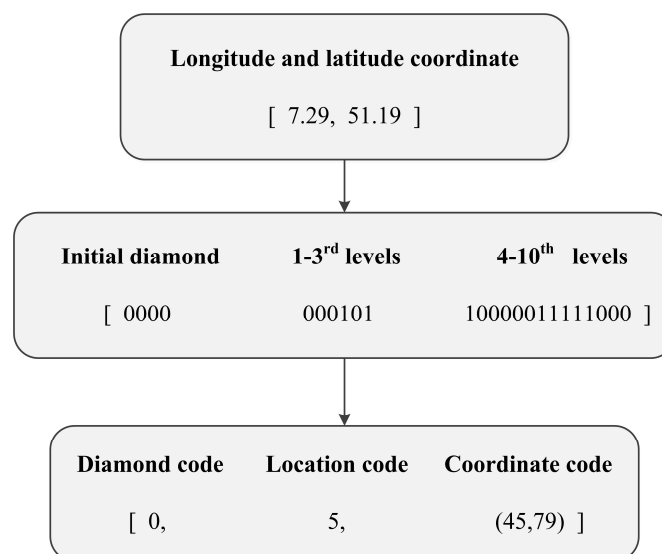


**Figure 9.** Diagram of coordinate transformation.

### 4. Algorithm Model Construction

#### 4.1. Airspace Representation

(1) Element information representation

- Working area: the area set by the airspace is set as a working area. The scope of the working area is composed of  $2n$  adjacent diamond areas of the same level as required. This paper takes a diamond area of the third level as an example, with an area of about  $800,000 \text{ km}^2$ . The number of the work area is represented by the 1–3rd levels of the grid, that is, the location code;
- Airspace: It is represented by the grid matrix at levels 4–10th. The grid surrounded by the four points of the coordinates of the boundary points of the airspace is the occupied grid of the airspace. Each airspace occupies the grid and expands one layer of the grid to obtain the airspace envelope. The initial 10 rhombus are level 0. According to the calculation formula of spherical arc length, the length of a single rhombus edge is about 7061 km. When dividing to level 10, the length of a single rhombus edge is about 7 km. The minimum distance of non-adjacent rhombus grids is one rhombus grid interval, that is, the vertical distance from the apex of the rhombus to the opposite side is about 6 km. During CD, the airspace is extended by one layer, that is, two surrounding layers are separated, and the minimum distance is 11.94 km, greater than 10 km. Therefore, the division to the 10th level not only meets the minimum safe separation distance of airspace, but also does not cause grid deformation in different latitude areas, and meets the accuracy conditions required for the use of the AR grid;
- Route: the width of the air route is 20 km, and the minimum is not less than 8 km. Therefore, the route can be regarded as a linear airspace model. As shown in Figure 10.

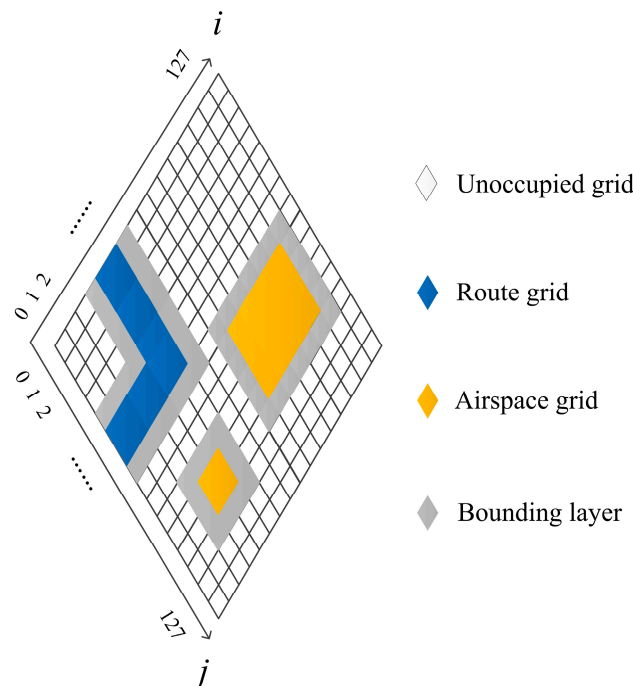


Figure 10. Schematic diagram of AR grid.

(2) Construction of airspace data matrix

- (a) The longitude and latitude coordinates of airspace boundary points are converted into spherical rectangular coordinates. The longitude and latitude coordinate  $G$  (longitude  $\lambda$ , latitude  $\varphi$ ), The equatorial radius of the Earth  $R$  corresponds to the three-dimensional rectangular coordinates  $C(X, Y, Z)$ . The relationship of transformation from longitude and latitude coordinates to

- spherical rectangular coordinates can be established from the spatial geometric relationship, as shown in Figure 5.
- (b) Spherical rectangular coordinate grid positioning. Given the grid vertex coordinates  $P_1, P_2, P_3, P_4$  and the coordinates of the point to be solved, connect the midpoint on the opposite side of the diamond grid to obtain the midpoint coordinates  $M_1, M_2, M_3, M_4$ . As shown in Figure 8, divide the grid into four quadrants, calculate the plane  $OM_1M_3$  normal vector  $\vec{v}_1$  and the plane  $OM_2M_4$  normal vector  $\vec{v}_2$ , and determine the quadrant of the point according to the relationship between the point and the plane. The initial state of Hilbert is State I. The Hilbert state of the next level is determined according to the quadrant transfer mode. Carry out hierarchical division until the 10th level. As shown in Figure 11.
  - (c) Airspace matrix construction. After connecting the four points of the coordinate code, the boundary of the airspace is obtained, the grid occupied by the airspace is calculated, and the value is assigned to 1, and the value of other grids in the mission area is assigned to 0, and a  $128 \times 128$  data matrix composed of 0 and 1 is obtained.
  - (d) Determination of airspace occupancy grid. Connect the coordinates of the airspace boundary points to obtain the airspace polygon, and determine whether all points in the matrix are within the airspace range. The value is assigned to 1 in the airspace range, and the value is 0 in the non-domain. The  $128 \times 128$  matrix composed of 0.1 is the airspace data matrix.

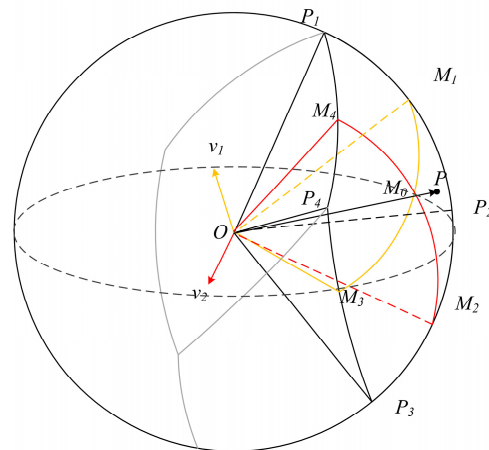


Figure 11. Position relationship between space normal vector and points.

As shown in Table 3, the corresponding relationship between the longitude and latitude coordinates of the boundary point of airspace A and the global codes is as follows:

Table 3. Correspondence between longitude and latitude coordinate and global code.

Longitude and Latitude Coordinate	Global Code	Diamond Code	Location Code	Coordinate Code
[113.46, 30.30]	[1-32-(52, 74)]	1	32	(52, 74)
[112.95, 29.77]	[1-32-(42, 73)]	1	32	(42, 73)
[113.57, 29.43]	[1-32-(47, 83)]	1	32	(47, 83)
[113.82, 29.99]	[1-32-(54, 81)]	1	32	(54, 81)

#### 4.2. Conflict Detection Method on the Base of Matrix Analysis

Hadamard product is a kind of operation of matrix, if  $A = \{a_{ij}\}$  and  $B = \{b_{ij}\}$  are two matrices of the same order, if  $c_{ij} = a_{ij} \times b_{ij}$ , then the matrix  $C = \{c_{ij}\}$  is the Hadamard product of A and B, recorded as  $A \circ B$ .

Given the boundary coordinates of the work area, the location code of the occupied grid can be obtained. Take the 3rd level diamond grid where the work area is located as the benchmark diamond and divide it to the 10th level. The benchmark diamond can be divided into 128 rows and 128 columns containing 16,384 diamond sub-grids. Think of the base diamond as  $128 \times 128$  matrix. Suppose there are airspace A and airspace B, and the longitude and latitude coordinates of airspace A and B are converted to the coordinates of boundary points  $(i, j)$  of A and B. Connect the coordinates of the boundary points to obtain the occupied grid of the airspace, assign the value to the occupied grid, and convert the geographic location of the airspace into the occupied grid of the matrix. The occupied coordinates of each airspace  $(i, j)$  are the row and column numbers of the matrix. The grid occupied by airspace A is assigned a value of  $a_{ij}$ , and other grids in the work area are assigned a value of 0, and the data matrix of airspace A,  $matA = \{a_{ij}\}$  is obtained; The grid occupied by airspace B is assigned a value of  $b_{ij}$ , and other grids in the work area are assigned a value of 0. The data matrix of airspace B,  $matB = \{b_{ij}\}$  is obtained  $128 \times 128$ .

The Hadamard product  $A \circ B = C$  operation is carried out to judge whether the assigned parameter in each row and column in the  $matC$  is 0. if the value of a row and column is  $c_{ij} = a_{ij} \times b_{ij}$ , it shows that the grid in row  $i$  and column  $j$  is occupied by airspace A and B at the same time, and the exact location of conflict is detected; if  $matC = O_{(i \times j)}$ , there is no conflict.

#### 4.3. Conflict Detection Model on the Base of Airspace Analysis

The airspace data is inputted into the database, and the airspace attribute includes time attribute T+ height attribute H+ range attribute R. Starting from the highest-level airspace group, judge the time attribute of airspace A and airspace B, C . . . If there is a conflict, set the airspace where there is a conflict to a collection of airspace. Judge the height attribute of airspace B and airspace C, D in turn. If there is a conflict, set the airspace where there is a conflict to another airspace collection. And so on, starting from the high-level airspace, the conflict is detected to the low-level airspace in turn, and the airspace where the conflict exists is set to a separate set of airspace. The CD process is shown in Figure 12:

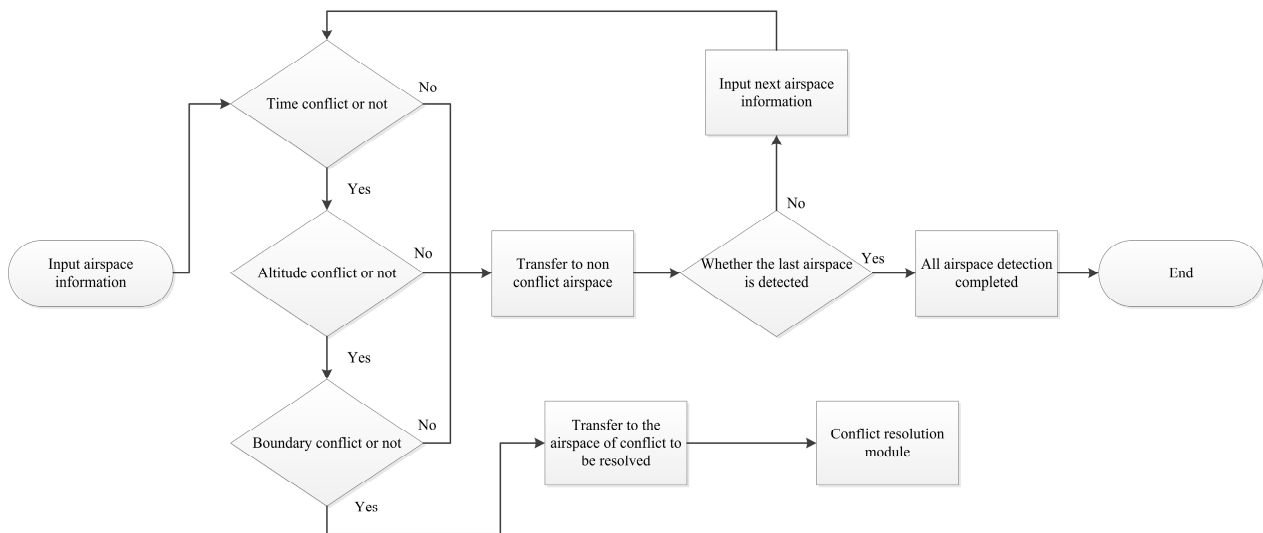


Figure 12. Airspace CD process.

- Step 1 time attribute CD. Compare the start time and end time of airspace A with other airspace. If there is a conflict with the intersection of the empty time, put the airspace An and the airspace with which there is a conflict into an airspace set;
- Step 2 height attribute CD. Logical relationship and time attribute detection: compare whether there is an intersection in the airspace altitude layer. After the CD of time and

height dimensions is completed, several airspace sets are obtained. There are both time conflicts and high conflicts in the airspace within these airspace sets;

- Step 3 range attribute CD. Obtain the data matrix of airspace A and the data matrix of airspace B. Carry on the Hadamard product operation  $matA \circ matB$  to obtain the  $matC$  of the same dimension. At that time  $matC = O_{(i \times j)}$ , it is determined that there is no conflict between airspace A and airspace B;

$$\begin{bmatrix} 1 & 1 & \dots & 0 & 0 \\ 1 & 1 & \dots & 0 & 0 \\ \vdots & \vdots & \ddots & \vdots & \vdots \\ 1 & 1 & \dots & 0 & 0 \\ 1 & 1 & \dots & 0 & 0 \end{bmatrix} \circ \begin{bmatrix} 0 & 0 & \dots & 1 & 1 \\ 0 & 0 & \dots & 1 & 1 \\ \vdots & \vdots & \ddots & \vdots & \vdots \\ 0 & 0 & \dots & 1 & 1 \\ 0 & 0 & \dots & 1 & 1 \end{bmatrix} = \begin{bmatrix} 0 & 0 & \dots & 0 & 0 \\ 0 & 0 & \dots & 0 & 0 \\ \vdots & \vdots & \ddots & \vdots & \vdots \\ 0 & 0 & \dots & 0 & 0 \\ 0 & 0 & \dots & 0 & 0 \end{bmatrix}$$

- Step 4 outputs the airspace CD results. Starting from the high-level airspace, it is detected in accordance with steps 1–3, and cycle to determine whether all airspace CD is completed.

### 5. Simulation Experiment

In a work area with boundary longitude and latitude coordinates: (108.10° E, 31.73° N), (114.05° E, 39.10° N), (118.85° E, 31.28° N), (113.14° E, 24.15° N), set 100 simulated airspace and routes as required to verify the feasibility of airspace conflict algorithm. Computer parameters for conducting simulation experiments: CPU:intel i5-10200H; Graphics card: GTX 3060 Laptop GPU; Memory: 16.0 GB; Running environment: Python 3.8 environment.

#### (1) Workspace and AR

According to the airspace boundary coordinates, the airspace occupation grid is determined, and the airspace number, priority, occupation time, altitude and other information are assigned to the grid. The airspace is entered in priority order, numbered from 001 to 100, and the routes occupancy grid is assigned a value of 5, so that the grid is occupied, and each airspace is surrounded by a layer for grid representation, as shown in Figure 13.

Routes and airspaces simulation diagram

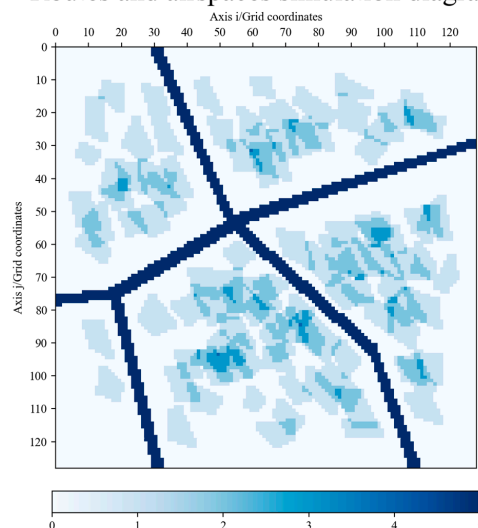


Figure 13. Routes and airspaces simulation diagram.

The airspace coordinates are entered in the Geographic Information System (GIS), and the AR is displayed simultaneously, as shown in Figure 14.



Figure 14. GIS simulation diagram.

(2) Perform airspace 3D CD

Run the CD algorithm based on matrix Hadamard product operation, and carry out the CD according to the time, height and range attributes of the airspace in order to verify the feasibility of the algorithm. As shown in Figure 15.

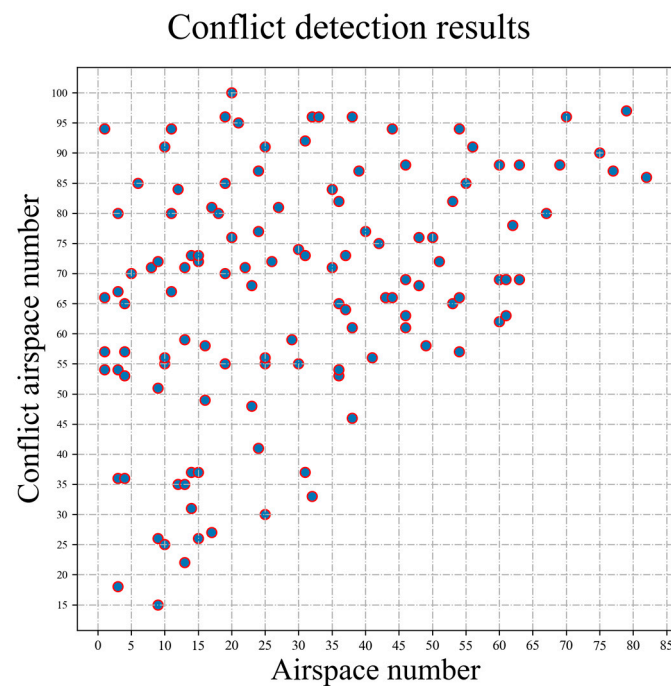


Figure 15. CD result.

(3) Simulation conclusion and analysis

According to the visualization simulation results, the airspace conflict point location and the corresponding airspace number of this conflict point location can be accurately derived. By comparing with the airspace delineated by GIS, the AG based on a spherical rhombus of the positive icosahedron is a rhombic grid, and there is some redundancy in the enclosing layers of the AG compared with the specified safety interval, but the airspace can still be accurately represented after the visualization of the rectangular grid to ensure the safety of CD. It is shown that the black-box algorithm is feasible.

Under the same experimental simulation conditions, using the Python language written by the traditional CD algorithm for comparison experiments. The collision detection time increases with the increase of the number of airspaces. Compared with the traditional algorithm, this algorithm is faster and more efficient.

When the number of airspace is 100, there are 88 airspace in conflict with other airspace, total of 120 conflict points. When using matrix detection algorithm for conflict detection, the detection time is 0.00288 s when the number of airspace is 10, and 0.20710 s when the number of airspace is 100; Using traditional detection algorithms for comparison, the detection time is 0.00287 s when the number of airspace is 10, and 0.27987 s when the number of airspace is 100. The amount of operations is  $1/2(n^2 + n)$ , the time complexity of the algorithm is  $O(n^2)$ , and the CD between hundreds of airspace is completed in seconds. As shown in Figure 16:

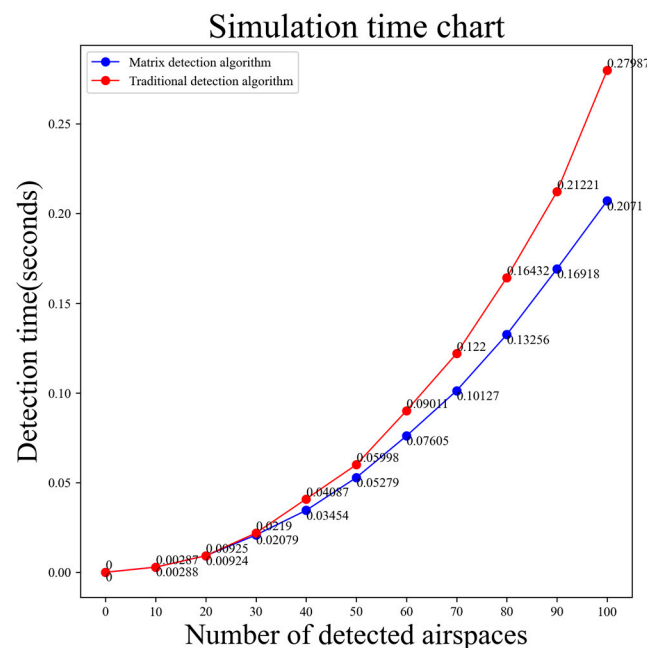


**Figure 16.** Simulation program run time.

The results show that the CD algorithm using the matrix Hadamard product operation can fully utilize the computer's GPU acceleration performance and improve the algorithm operation efficiency.

The implementation parameters of the algorithm are longitude and latitude coordinates of airspace, occupation height information of airspace, time information, and the custom sequence number of airspace.

## 6. Conclusions

Based on the characteristics of air demand, this paper designs the subdivision scheme and the spatial coordinate coding structure based on the regular icosahedral spherical rhombus discrete grid model, realizes the subdivision level most suitable for the AR, overcomes the grid deformation problem in different latitudes, and ensures the accuracy of the AR. The method of transforming longitude and latitude coordinates into global positioning codes and the process of AG representation are designed. Compared with the traditional AR method, the representation method of airspace data matrix based on the regular icosahedral spherical rhombus discrete grid is more convenient. Each grid corresponds to a unique code, which converts the spatial location into the occupied grid, and finally boils down to the operation between the airspace data matrices.

This method is a "black-box algorithm", that is, the operator will input the longitude and latitude coordinates, using a diamond grid algorithm to calculate and derive CD

results, the process is not displayed in the operating interface, but directly for the user output results. It effectively shortens the program's running time and improves detection efficiency. In the case of large-scale use of space, it can achieve fast, efficient, and accurate detection of conflicts.

**Author Contributions:** Conceptualization, G.Z.; Formal analysis, K.Q.; Investigation, L.T. and Y.W.; Methodology, G.Z.; Resources, Y.W. and L.T.; Software, K.Q.; Supervision, G.Z. and Y.W.; Visualization, K.Q.; Writing—original draft, K.Q.; Writing—review & editing, G.Z.; funding acquisition, K.Q. All authors have read and agreed to the published version of the manuscript.

**Funding:** This research received no external funding.

**Institutional Review Board Statement:** Not applicable.

**Informed Consent Statement:** Not applicable.

**Data Availability Statement:** Not applicable.

**Conflicts of Interest:** The authors declare no conflict of interest.

## Abbreviations

AG	Airspace Grid
AR	Airspace Representation
CD	Conflict Detection
GIS	Geographic Information System

## References

- Sahr, K.; White, D.; Kimerling, A.J. Geodesic discrete global grid systems. *Cartogr. Geogr. Inf. Sci.* **2003**, *30*, 121–134. [\[CrossRef\]](#)
- White, D. Global grids from recursive diamond subdivisions of the surface of an octahedron or icosahedrons. *Environ. Monit. Assess.* **2000**, *64*, 93–103. [\[CrossRef\]](#)
- Gregory, M.J.; Kimerling, A.J.; White, D.; Sahr, K. A comparison of intercell metrics on discrete global grid systems. *Comput. Environ. Urban Syst.* **2008**, *32*, 188–203. [\[CrossRef\]](#)
- Ben, J.; Tong, X.C.; Zhang, Y.S.; Chen, R.G. Research on algorithms and software models for generating spherical isoparametric grid systems. *J. Surv. Mapp.* **2007**, *2*, 187–191.
- Zhou, L.C.; Sheng, Y.H.; Lin, B.S.; Lü, G.N.; Zhao, Z.P. Spherical rhombic discrete grid positive icosahedron profile method. *J. Surv. Mapp.* **2014**, *43*, 1293–1299.
- Lin, B.X.; Xu, D.P.; Sheng, Y.H.; Lü, G.N.; Zhou, L.C. Coding model of ortho-icosahedral spherical rhombic discrete grid and its mapping method. *J. Surv. Mapp.* **2016**, *45* (Suppl. S1), 23–31.
- Jardin, M. Grid-based strategic air traffic conflict detection. In *Proceedings of the AIAA Guidance, Navigation, and Control Conference and Exhibit, San Francisco, CA, USA, 15–18 August 2005*; ARC: Reston, VA, USA, 2005; p. 5826.
- Ruiz, S.; Piera, M.; Zúñiga, C. Relational Time-Space Data Structure to Speed Up Conflict Detection under Heavy Traffic Conditions; First SESAR Innovation Days: Sabadell, Spain, 2011; pp. 1–8.
- Kuenz, A. A global airspace model for 4D-trajectory-based operations. In *Proceedings of the IEEE/AIAA 30th Digital Avionics Systems Conference, Piscataway, NY, USA, 16–20 October 2011*; pp. 3E3-1–3E3-9.
- Miao, S.; Cheng, C.; Zhai, W.; Ren, F.; Zhang, B.; Li, S.; Zhang, J.; Zhang, H. A low-altitude flight conflict detection algorithm based on a multilevel grid spatiotemporal index. *Int. J. Geo-Inf.* **2019**, *8*, 289. [\[CrossRef\]](#)
- Liu, Z.Q.; Nan, Y.; Xie, R.H. Airspace conflict detection method based on profiling grid. *Nav. Electron. Eng.* **2022**, *42*, 157–162.
- Gong, W.; Tao, D.J.; Yan, J.M. Research on airspace conflict detection and deconfliction technology based on raster model. *Inf. Technol. Res.* **2021**, *47*, 46–50.
- Sui, D.; Zhang, K. A Tactical Conflict Detection and Resolution Method for En-Route Conflicts in Trajectory-Based Operations. *J. Adv. Transp.* **2022**, *2022*, 9283143. [\[CrossRef\]](#)
- Cai, M.; Wan, L.J.; Gao, C.Z.; Xu, X.Y. GJK-based airspace conflict detection algorithm in spatial grid system. *J. Xihua Univ. (Nat. Sci. Ed.)* **2022**, *41*, 36–41.
- Zhou, X.M.; Tang, D.J.; Hao, L.Z.; Song, Y.C. Application of geodesic grid theory in image processing. *Mapp. Sci.* **2019**, *44*, 84–89.
- Zhao, X.S.; Wang, L.; Wang, H.B.; Li, Y. Modeling methods and fundamental issues of global discrete grid. *Geogr. Geogr. Inf. Sci.* **2012**, *28*, 29–34.
- Cheng, C.Q.; Wu, F.L.; Wang, R.; Qin, Y.G.; Tong, X.C. A preliminary investigation on the construction of geospatial reference grid system. *J. Peking Univ. (Nat. Sci. Ed.)* **2016**, *52*, 1041–1049.
- Ben, J. *Research on the Theory and Algorithm of Discrete Grid Data Model for Geospatial Information*; Chinese People's Liberation Army Information Engineering University: Zhengzhou, China, 2005.

19. Zhang, Y.M.; Chen, W.H.; Nie, H.S.; Li, T.G.; Zeng, S.Q. Research on recursive profiling method for spherical rhombic grid. *Geogr. Geogr. Inf. Sci.* **2010**, *26*, 34–37.
20. Zhao, X.S.; Ben, J.; Sun, W.B.; Tong, X.C. A review of research progress on geo-profile grids. *J. Surv. Mapp.* **2016**, *45* (Suppl. S1), 1–14.
21. Goodchild, M.F. Geographical Information Science. *International. J. Geogr. Inf. Syst.* **1992**, *6*, 31–45.
22. Sun, W.B.; Zhao, X.S.; Gao, Y.L.; Wang, H.B. Profiling method and feature analysis of spherical seemingly uniform grid. *Geogr. Geogr. Inf. Sci.* **2009**, *25*, 53–56+60.
23. Lin, C. *Research on Spherical Rhombic Mesh Dissection, Coding and Data Integration*; Jiangxi University of Technology: Nanchang, China, 2013.
24. Goodchild, M.F.; Guo, H.; Annoni, A.; Bian, L.; Bie, K.; Campbell, F.; Craglia, M.; Ehlers, M.; Genderen, J.; Jackson, D. Next-generation digital earth. *Proc. Natl. Acad. Sci. USA* **2012**, *109*, 11088–11094. [[CrossRef](#)]
25. Fekete, G.; Treinish, L. Sphere Quadtrees: A New Data Structure to Support the Visualization of Spherically Distributed Data. *Extracting. Mean. Complex Data Process. Disp. Interact.* **1990**, *1259*, 242–253.
26. Fan, D.W.; He, B.L.; Li, C.H.; H, J.; Xu, Y.F. Comparison of spherical distance calculation methods and accuracy. *Astron. Res. Technol.* **2019**, *16*, 69–76.
27. Zhou, Y.; Zhu, Q.; Zhang, Y.T. Spatial data partitioning method based on Hilbert curve hierarchical decomposition. *Geogr. Geogr. Inf. Sci.* **2007**, *4*, 13–17.
28. Lu, F.; Zhou, C.; Hu, A. Hilbert code generation algorithm based on spatial hierarchical decomposition. *Chin. J. Graph. Graph.* **2001**, *5*, 59–63.

**Disclaimer/Publisher’s Note:** The statements, opinions and data contained in all publications are solely those of the individual author(s) and contributor(s) and not of MDPI and/or the editor(s). MDPI and/or the editor(s) disclaim responsibility for any injury to people or property resulting from any ideas, methods, instructions or products referred to in the content.